Co-doped zigzag graphene nanoribbon based gas sensor for sensitive detection of H₂S: DFT study

Ehab Salih [a], Ahmad I. Ayesh [a,b,*]

[a] Department of Mathematics, Statistics and Physics, Qatar University, P. O. Box 2713, Doha, Qatar
[b] Center for Sustainable Development, Qatar University, P. O. Box 2713, Doha, Qatar

ABSTRACT

In this work, we present a highly sensitive gas sensor for the detection of poisonous hydrogen sulfide gas (H₂S) based on copper and zinc co-doped zigzag graphene nanoribbon (Cu/Zn-ZGNR). The electronic properties as well as the sensing performance of Cu/Zn-ZGNR toward H₂S were investigated employing density functional theory (DFT). The adsorption capacity of the newly developed Cu/Zn-ZGNR system was compared with both pristine ZGNR as well as doped Zn-ZGNR and Cu-ZGNR systems. The adsorption energy (E_{ads}) of H₂S/Zn-ZGNR and H₂S/Cu-ZGNR systems were found to be −2.237 and −1.129 eV, respectively. For the case of H₂S/Cu/Zn-ZGNR, the adsorption energy (E_{ads}) and charge transfer (Δq) reflected an outstanding increase to −7.043 eV and −0.311 e, respectively, when compared with both pristine and doped systems: ZGNR, Zn-ZGNR, and Cu-ZGNR. Moreover, the adsorption distance (D) between H₂S and Cu/Zn-ZGNR decreased remarkably to 2.23 Å and an S–Cu bond was generated. The response towards H₂S of the developed ZGNR, Zn-ZGNR, Cu-ZGNR, and Cu/Zn-ZGNR gas sensors has been investigated as well. Particularly, the response of H₂S to Cu/Zn-ZGNR system demonstrated a significant high value of 48.92%. Therefore, the newly developed co-doped Cu/Zn-ZGNR based gas sensor can be recommended as a highly sensitive H₂S sensor.

1. Introduction

In the recent two decades, graphene as a superior two-dimensional material, has revealed a considerable performance in the field of gas sensors [1–3] owing to its magnificent thermal, mechanical, and electrical characteristics [4–6]. Among the various forms of graphene-based materials, the qausi one-dimensional form, which is called graphene nanoribbon (GNR), has been examined as a gas sensor for the detection of different toxic gases [7–11]. Counting on the carbon atoms arrangement at the edges, GNR is categorized into zigzag and armchair graphene nanoribbon [12–15]. The preference of GNR in the sensing applications is mostly attributed to the controllable band gap and the existence of the edges that act as chemically active sites, which assist in the interaction with the gas molecules [16].

The toxic hydrogen sulfide (H₂S) gas has been chosen to be the target gas of the current study due to the dangerous effects that it causes to the human respiratory and nervous systems [17–19]. It is a poisonous and very flammable gas at the higher concentrations and generated mostly from the decomposition of organic matter as well as the petroleum extraction [20]. Various investigations have been reported recently about using GNR as a gas sensor to detect the poisonous H₂S gas molecules. For example, a comparative study

between the performance of zigzag and armchair graphene nanoribbons toward the detection of H_2S was published recently [21]. The researchers of this work demonstrated that the zigzag graphene nanoribbon is more sensitive for the detection of H_2S as compared with the armchair graphene nanoribbon. Moreover, very recently, a comparative investigation between the sensitivity toward H_2S gas of three graphene-based materials was reported [22]. In the study, graphene-nanosheet, armchair graphene-nanoribbon, and zigzag graphene-nanoribbon were utilized for the purpose of detection of H_2S gas. The results of this work revealed that functionalizing the three forms of graphene-based materials with –O– or –OH functional groups have a considerable impact on the adsorption parameters with the best performance observed for the case of hydroxyl modified ZGNR. Consequently, the ZGNR was considered as the substrate of the current study for the sensitive detection of H_2S. Furthermore, different investigations were reported in recent years showing the impact of doping graphene-based materials on their accomplishment in the detection of various poisonous gases [23–27].

In the current study, copper and zinc co-doping of ZGNR (Cu/Zn-ZGNR) have been investigated theoretically for the purpose of enhancing its performance towards the sensing of H_2S gas. To the best of our knowledge, this is the first time in literature where Cu/Zn co-doped ZGNR is built and utilized to sense H_2S gas using simulation based on density functional theory (DFT). The results reveal that the sensitivity of the established Cu/Zn-ZGNR system toward the detection of the poisonous H_2S gas is evidently improved as compared with both pristine and doped systems: ZGNR, Zn-ZGNR, and Cu-ZGNR. Thus, Cu and Zn co-doping of ZGNR can be considered as a promising method to enhance its performance towards the sensitive detection of the poisonous H_2S gas molecules.

2. Computational details

The electronic properties, as well as the sensing performance of pristine and doped systems (ZGNR, Zn-ZGNR, Cu-ZGNR, and Cu/Zn-ZGNR) toward H_2S gas were investigated employing Atomistic ToolKit Virtual NanoLab (ATK-VNL) package (version 2018.06). In order to define the exchange correlation function, the generalized gradient approximation combined with the Perdew-Burke-Ernzerhof, that is abbreviated as (GGA-PBE), were employed [28,29]. For the purpose of correcting the influence of van der Waals interactions, DFT-D2 of Grimme has been utilized [29–32]. The (LBFGS) optimizer has been employed in order to attain the most stable adsorption configurations for the built systems [33]. Thus, all the established ZGNR, Zn-ZGNR, Cu-ZGNR, and Cu/Zn-ZGNR systems with and without the existence of the H_2S gas were optimized until a 0.05 eV/Å force convergence was attained. The energy mesh cutoff is set to be 150 Ry, stress error tolerance of 0.1 GPa has been utilized during the calculations, and a $4 \times 4 \times 1$ k point sampling has been employed for Brillouin-zone integration. To confirm the adsorption of H_2S on any of the developed ZGNR, Zn-ZGNR, Cu-ZGNR, and Cu/Zn-ZGNR sensors, the adsorption energy was illustrated employing equation (1) [34,35]:

$$E_{ads} = E_{Cu/Zn-ZGNR+H_2S} - E_{Cu/Zn-ZGNR} - E_{H_2S} \tag{1}$$

where refers to the total energy of the relaxed H_2S adsorbed on any of developed ZGNR, Zn-ZGNR, Cu-ZGNR, and Cu/Zn-ZGNR sensors, $E_{Cu/Zn-ZGNR}$ refers to the total energy of any of developed sensors prior to the interaction with H_2S, and E_{H_2S} is to the total energy of the relaxed H_2S gas. In addition, the mechanism of the transfer of the charge among the H_2S gas molecules and the built ZGNR, Zn-ZGNR, Cu-ZGNR, and Cu/Zn-ZGNR sensors has been demonstrated employing Mulliken population method with the aid of equation (2) [35, 36]:

$$\Delta q = q_a - q_p \tag{2}$$

where, q_a corresponds to the Mulliken charges of H_2S molecules after being adsorbed on any of the developed ZGNR, Zn-ZGNR, Cu-ZGNR, and Cu/Zn-ZGNR sensors, while q_p is the Mulliken charges of the relaxed H_2S prior the interaction with any of the established sensor materials. For the current-voltage characteristics, the semi-empirical extended Hückel model was used and k-point sampling of $1 \times 1 \times 5$ has been utilized. The total current passing through the established ZGNR, Zn-ZGNR, Cu-ZGNR, and Cu/Zn-ZGNR devices has been evaluated with the aid of Landauer–Büttiker formula [37]:

$$I = \frac{2e}{h} \int T(E, V)[f(E - \mu_L) - f(E - \mu_R)]dE \tag{3}$$

where $T(E, V)$ and f refer to the transmission function and the Fermi distribution function, respectively. While, μ_L and μ_R correspond to the electrochemical potential of the left and the right electrodes, respectively. With the aid of the current-voltage curves, the response (R (%)) of the sensor towards the toxic H_2S gas molecules was elucidated utilizing equation (4) [38–40]:

$$R\,(\%) = \left| \frac{I - I_o}{I_o} \right| x100\% \tag{4}$$

where I refers to the current of any of the built devices after adsorbing H_2S gas and I_o is the current of any of the devices without interacting with the H_2S gas.

3. Results and discussion

Copper and zinc co-doped zigzag graphene nanoribbon (Cu/Zn-ZGNR) is built using a first principles based simulation, and then utilized to detect H_2S gas with improved sensitivity. In order to confirm the impact of co-doping with Cu and Zn on the response of ZGNR toward the detection of H_2S, the performance of the new system was compared with those of ZGNR, Zn-ZGNR, and Cu-ZGNR
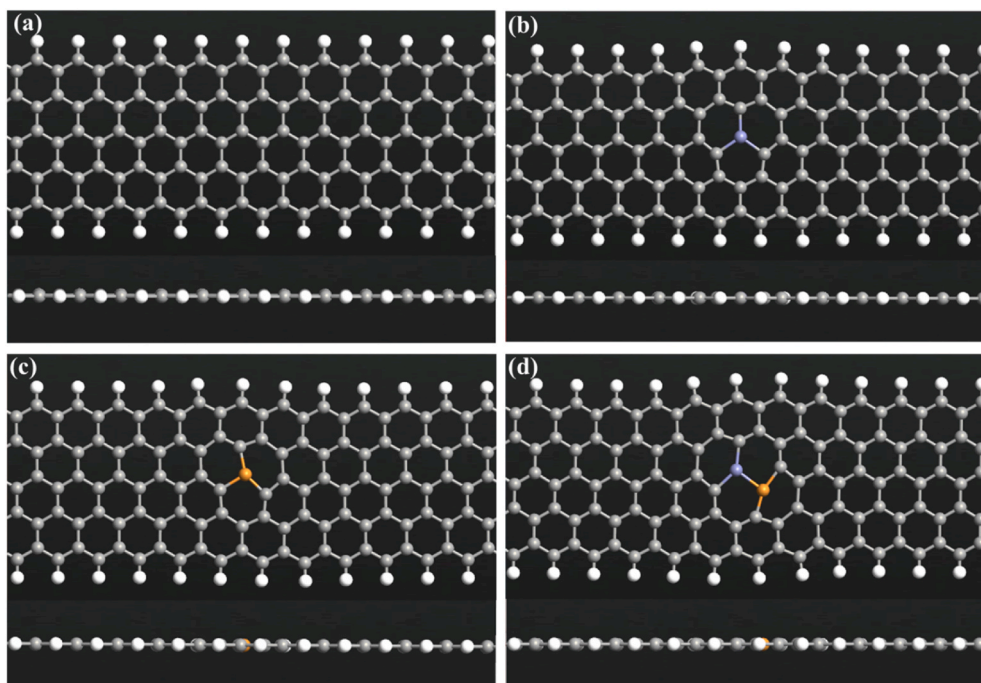
Fig. 1. Top and side views of the relaxed a) ZGNR, b) Zn-ZGNR, c) Cu-ZGNR, and d) Cu/Zn-ZGNR.
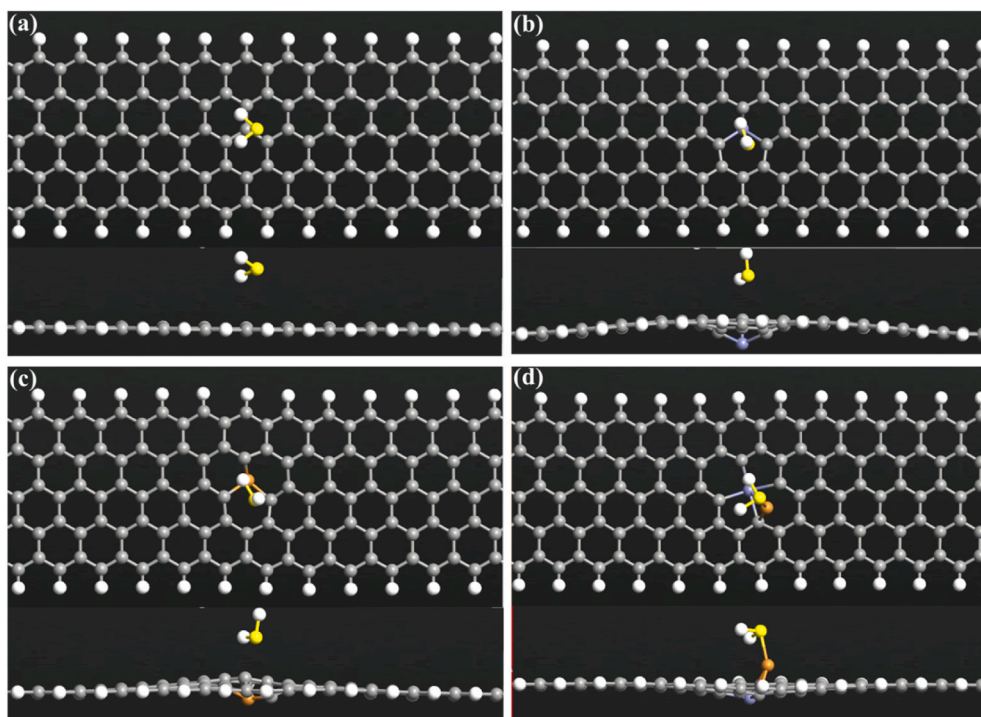

Fig. 2. Top and side views of the relaxed a) H_2S/ZGNR, b) H_2S/Zn-ZGNR, c) H_2S/Cu-ZGNR, and d) H_2S/Cu/Zn-ZGNR.

systems. The established ZGNR, Zn-ZGNR, Cu-ZGNR, and Cu/Zn-ZGNR systems prior and after the interaction with H_2S are relaxed to acquire the most stable adsorption configuration as shown in Figs. 1–2. The geometrical parameters of ZGNR, Zn-ZGNR, Cu-ZGNR, and Cu/Zn-ZGNR systems are listed in Table 1. Upon the relaxation, the results reflect that the average length of the C–C and C–H bonds of ZGNR are 1.43 and 1.10 Å, respectively. For the cases of Zn-ZGNR and Cu-ZGNR systems, the average C–Zn and C–Cu bond lengths are
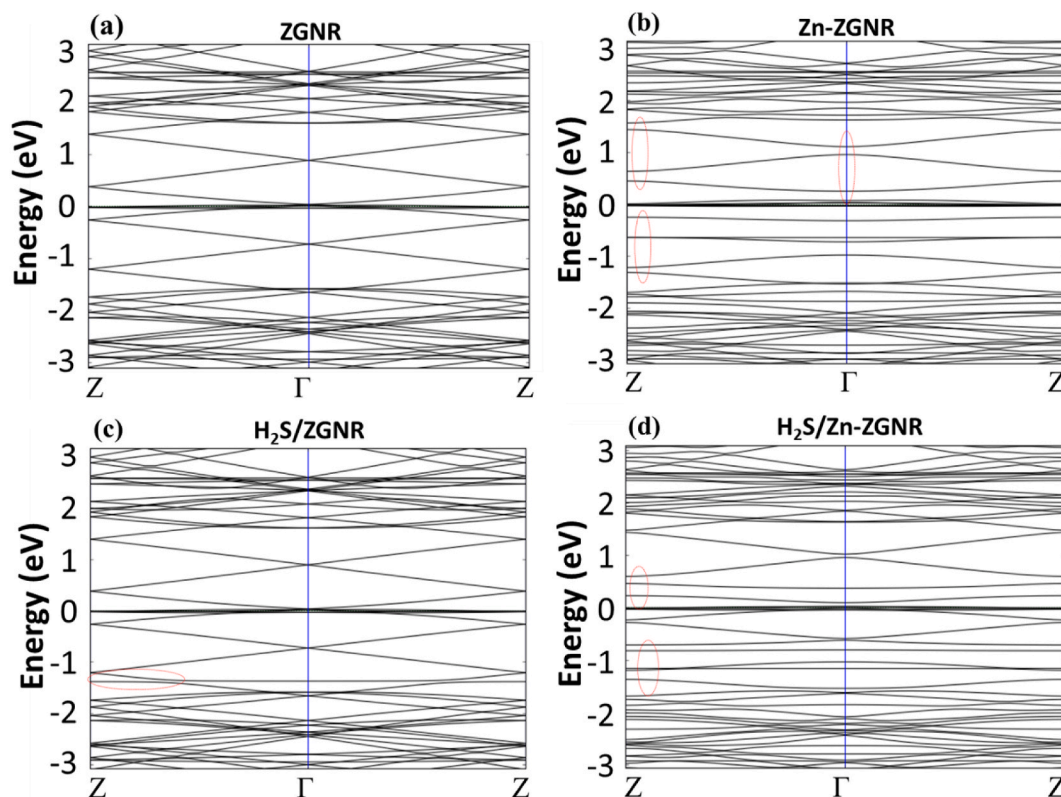
Table 1

Geometrical parameters of ZGNR, Zn-ZGNR, Cu-ZGNR, and Cu/Zn-ZGNR.

System	Bond length (Å)				
	C–C	C–H	C–Zn	C–Cu	Cu–Zn
ZGNR	1.43	1.10	–	–	–
Zn-ZGNR	1.38[a]	1.10	1.77	–	–
Cu-ZGNR	1.39[a]	1.10	–	1.73	–
Cu/Zn-ZGNR	1.39[a]	1.10	1.79	1.73	2.03

[a] Close to the position of the metal atoms.

Table 2

Adsorption distance (D), charge transfer (Δq), and adsorption energy (E_{ads}) of H_2S/ZGNR, H_2S/Zn-ZGNR, H_2S/Cu-ZGNR, and H_2S/Cu/Zn-ZGNR systems.

System	D (Å)	Δq (e)	E_{ads} (eV)
H_2S/ZGNR	3.24	−0.022	−0.364
H_2S/Zn-ZGNR	2.70	−0.037	−2.237
H_2S/Cu-ZGNR	2.75	−0.059	−1.129
H_2S/Cu/Zn-ZGNR	2.23	−0.311	−7.043

Fig. 3. Band structures of a) ZGNR, b) Zn-ZGNR, c) H_2S/ZGNR, and d) H_2S/Zn-ZGNR.

1.77 and 1.73 Å. Meanwhile, the average length of C–Zn, C–Cu, and Cu–Zn bonds of Cu/Zn-ZGNR are 1.79, 1.73, and 2.03 Å as listed in Table 1. Furthermore, the average length of the immediate C–C bonds close to the position of the metal atoms decreases to 1.38 Å for the case of Zn-ZGNR and 1.39 Å for both Cu-ZGNR and Cu/Zn-ZGNR systems. After the optimization, the H_2S molecule changes its direction in which one H and the sulfur atoms face the plane of the ribbon for the cases of H_2S/ZGNR, H_2S/Zn-ZGNR, and H_2S/Cu-ZGNR systems as shown in Fig. 2(a)–2(c). Nevertheless, the smallest distance is detected between the H atom and the systems. Meanwhile, a little bending in the ribbon toward the gas is observed for the cases of the H_2S/Zn-ZGNR and H_2S/Cu-ZGNR systems. Upon the adsorption of H_2S on Cu/Zn-ZGNR system (Fig. 2(d)), the Zn atom becomes bonded with four C atoms from the ribbon. Meanwhile, the Cu atom is protruded toward the H_2S gas with two bonds between the Zn atom and one C atom from the ribbon and
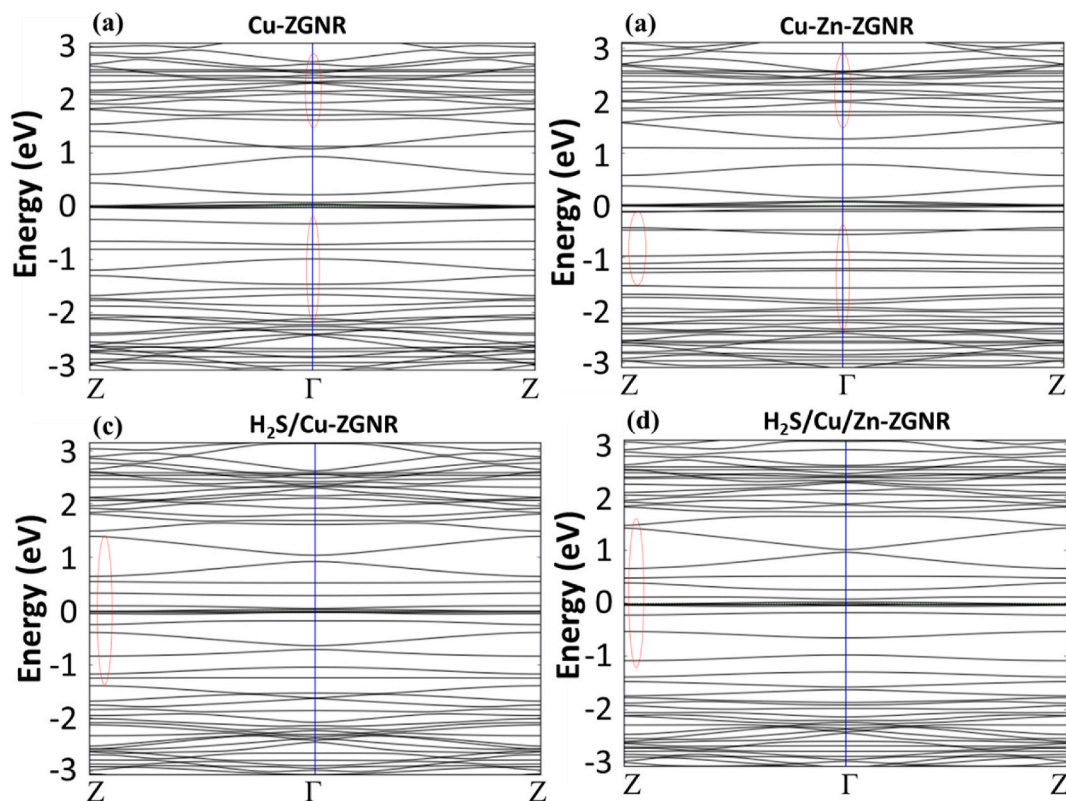
Fig. 4. Band structures of a) Cu-ZGNR, b) Cu/Zn-ZGNR, c) H_2S/Cu-ZGNR, and d) H_2S/Cu/Zn-ZGNR.

another bond with length 2.23 Å with the S atom of the gas. Consequently, the average lengths of C–Zn, C–Cu, and Cu–Zn bonds increase to 2.00, 2.07, and 2.52 Å.

The adsorption distance (D), Δq, and E_{ads} of H_2S/ZGNR, H_2S/Zn-ZGNR, H_2S/Cu-ZGNR, and H_2S/Cu/Zn-ZGNR systems are calculated and listed in Table 2 to prove the successful detection of the gas. The results show that, the adsorption distance, charge transfer, and the adsorption energy for the case of the H_2S/ZGNR system are 3.24 Å, −0.022 e, and −0.364 eV, respectively. These results indicates that the H_2S gas is physisorbed on the surface of ZGNR [41]. A considerable improvement in the adsorption parameters is noticed after doping ZGNR with Zn and Cu. For instance, the adsorption energy increases to −2.237 and −1.129 eV, while the adsorption distance decreases to 2.70 and 2.75 Å for the cases of H_2S/Zn-ZGNR and H_2S/Cu-ZGNR systems, respectively. Besides, the amount of charges that transfer from the gas to the systems reveal higher values after doping ZGNR with any of the Zn or Cu atoms. Upon co-doping ZGNR with Cu and Zn, the adsorption parameters demonstrate an outstanding improvement as compared with the pristine and doped ZGNR, Zn-ZGNR, and Cu-ZGNR systems. On one hand, the adsorption distance decreases to 2.23 Å and the charge transfer increases significantly to −0.311e. On the other hand, the adsorption energy increases outstandingly to −7.034 eV. This value is nearly 19 times larger than the case of H_2S/ZGNR system, while it is almost 3 and 6 times larger than the cases of H_2S/Zn-ZGNR and H_2S/Cu-ZGNR, respectively. The magnificent increase in the adsorption energy as well as the charge transfer of H_2S/Cu/Zn-ZGNR is attributed to the formation of the S–Cu bond that is observed after the adsorption of H_2S on the Cu/Zn-ZGNR system as shown in Fig. 2 (c). The obtained results for this case demonstrate that H_2S molecule is chemisorbed on the surface of Cu/Zn-ZGNR system [41].

The band structure results of ZGNR, Zn-ZGNR, Cu-ZGNR, and Cu/Zn-ZGNR systems prior and after the detection of H_2S are illustrated in Figs. 3–4. The results show that the bandgap of ZGNR (Fig. 3(a)) is zero demonstrating its metallic nature that has been reported [42,43]. After doping ZGNR with Zn, some variations are noticed close to Fermi level in the valence and the conduction bands. For instance, the spaces between the bands close to Fermi level (from 0 to ±2 eV) increase slightly in addition to the appearance of new flat bands between 0 and -1 eV as shown in Fig. 3(b). The same trend is almost observed as well for the cases of Cu-ZGNR and Cu/Zn-ZGNR (Fig. 4(a) - 4(b)) besides a flattening to some of the valence and the conduction bands upon introducing the Cu and Zn atoms to the surface of the ribbon. Fig. 3(c) shows the band structure of H_2S/ZGNR system. The figure demonstrates the appearance of a new band in the valence bands (between −1 and −2 eV) as a result of the interaction between the H_2S gas and the ZGNR system. For the case of the H_2S/Zn-ZGNR system (Fig. 3(d)), new bands that are not existed in the band structure of Zn-ZGNR are observed close to Fermi level. The same trend is noticed as well for the cases of the H_2S/Cu-ZGNR and H_2S/Cu/Zn-ZGNR systems as shown in Fig. 4(c) - 4 (d). The band structure results that are obtained in the current study reveal that doping as well as co-doping ZGNR affect its electronic characteristics. Furthermore, once the H_2S gas is adsorbed on the surface of any of the developed systems, noticeable modifications including the appearance of new bands are demonstrated. These modifications are likely to illustrate new electronic states creation as a
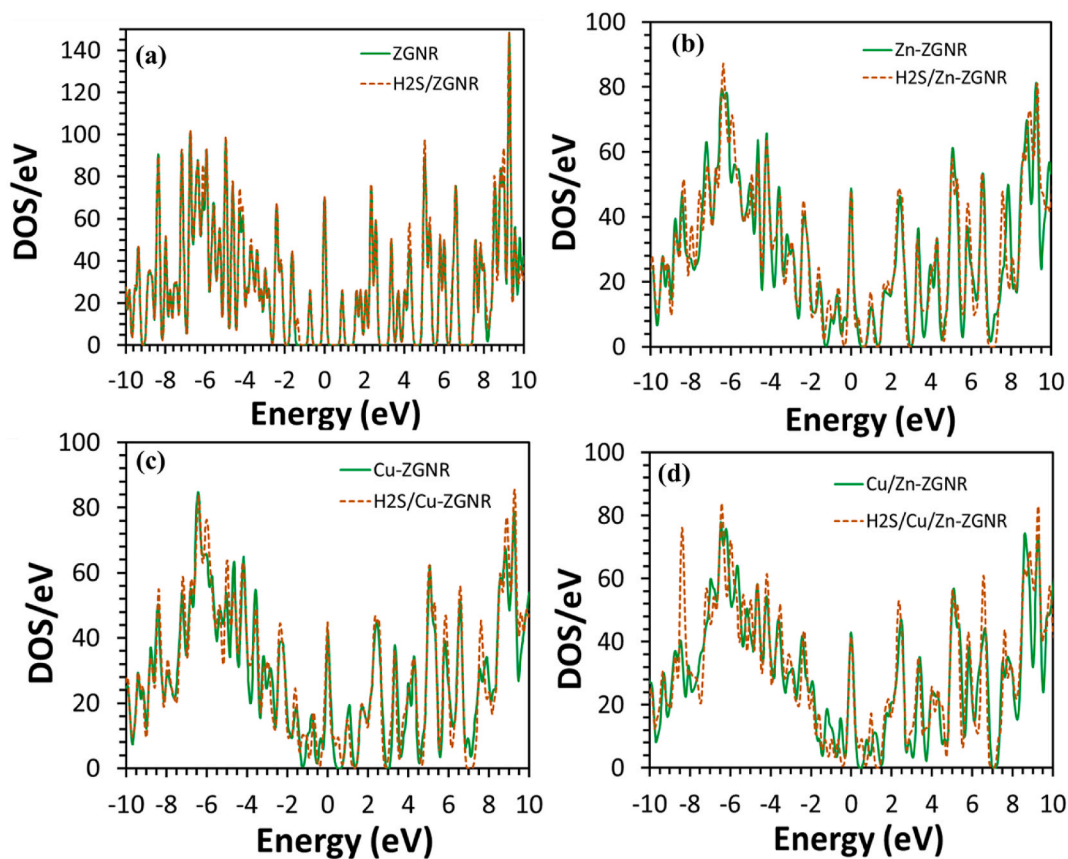
Fig. 5. Density of states of a) ZGNR, b) Zn-ZGNR with and without the existence of H_2S, c) Cu-ZGNR, and d) Cu/Zn-ZGNR with and without the existence of H_2S.

result of the interaction with the H_2S gas molecules [44].

To further understand the impact of doping and co-doping ZGNR on the electronic properties, the density of states of the pristine ZGNR, Zn-ZGNR, Cu-ZGNR, and Cu/Zn-ZGNR systems are investigated as shown in Fig. 5 (as well as in Fig. 1 of the supplement material). The highest intensity for the peak at Fermi level is observed for the case of pristine ZGNR as compared with the other three modified systems. Furthermore, remarkable variations as well as new peaks are observed in the valence and the conductions bands upon doping and co-doping ZGNR, which further confirm the band structure results. To verify the successful adsorption of H_2S on the surface the ZGNR, Zn-ZGNR, Cu-ZGNR, and Cu/Zn-ZGNR systems, the density of states of these systems with and without the gas are investigated and shown in Fig. 5. As shown in Fig. 5(a), the changes of the density of states are not significant upon the adsorption of H_2S on the surface of pristine ZGNR. Therewith, the peaks around −6.08, −4.26, 4.24, 5.03, and 9.01 eV demonstrate a slight increase. Besides, a new peak is observed around −1.35 eV, which is in excellent agreement with the appearance of new band in this range in the band structure of H_2S/ZGNR systems (Fig. 3(c)). After doping and co-doping ZGNR with Cu and Zn atoms, the impact of the H_2S adsorption on the density of states become more noticeable as compared with the case of pristine ZGNR. For instance, the density of states around −6.36, −5.90, −1.07, 1.00, and 5.80 eV increase upon adsorption of H_2S on the surface of Zn-ZGNR (Fig. 5(b)). In addition, three new peaks around −7.95, −7.53, and 0.43 eV are observed and the peak around 7.81 eV is shifted to 7.60 eV. For the case of H_2S/Cu-ZGNR (Fig. 5(c)), the density of states results demonstrate an increase in the peaks around −5.97, −4.98, −2.38, −1.63, 5.31, 5.80, 7.64, and 8.86 eV as compared with Cu-ZGNR in addition to the appearance of two new peaks around 0.56 and 9.63 eV. The highest impact of the adsorption of H_2S gas on the density of states is observed for the case Cu/Zn-ZGNR (Fig. 5(d)) system due to the protruding of the Cu atom and the formation of S–Cu bond. On one hand, the density of states around −8.36, −4.17, −3.49, −3.05, −1.59, 2.37, 5.78, 6.58, 7.61, and 9.26 eV increase considerably after the adsorption of H_2S. On the other hand, the peaks in the range from −6.41 to −5.00 eV shift to higher values and the two peaks around 0.86 and 1.06 eV are shifted to 0.54 and 1.00 eV to be closer to Fermi level. The prominent variations in the density of states in the valence and the conductions bands for the cases of H_2S/Zn-ZGNR, H_2S/Cu-ZGNR, and H_2S/Cu/Zn-ZGNR systems as compared with the pure systems reveal a change in the number of occupied states upon the gas adsorption [45,46]. These results confirm that the poisonous H_2S gas is successfully adsorbed on the surface of Zn-ZGNR, Cu-ZGNR, and Cu/Zn-ZGNR systems.

The electron transport properties of the present ZGNR, Zn-ZGNR, Cu-ZGNR, and Cu/Zn-ZGNR sensors are examined using current-voltage (I(V)) characterization. The two probe device structure of the developed ZGNR sensor is shown in Fig. 6(a), where the sizes of
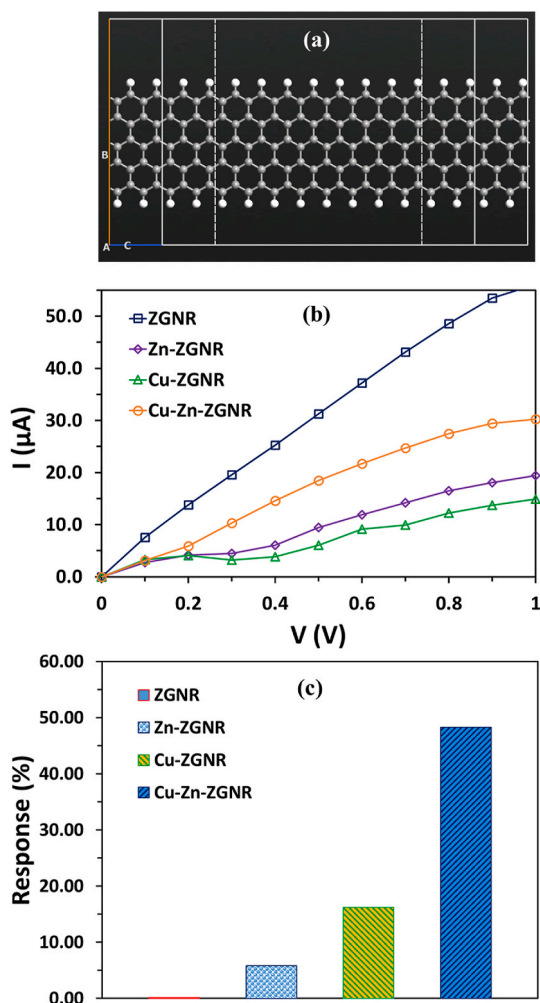
Fig. 6. a) Two probe device for ZGNR, b) I(V) curves of the ZGNR, Zn-ZGNR, Cu-ZGNR, and Cu/Zn-ZGNR systems, and b) response of H_2S for the established ZGNR, Zn-ZGNR, Cu-ZGNR, and Cu/Zn-ZGNR sensors.

Table 3
Comparison between previous results for H_2S adsorption on different modified graphene systems and the results obtained in this work for adsorption energy, adsorption distance, and charge transfer of Cu/Zn-ZGNR systems.

System	E_{ads} (eV)	D (Å)	Δq (e)	Reference
P-graphene	− 0.244	4.09		[44]
Si-graphene	− 0.259	3.65		
S-graphene	− 0.420	3.735		[48]
Ni-graphene	− 0.699	2.426	0.233	[49]
OH-graphene	− 1.263	2.412	0.054	
Ni-graphene	− 0.97	2.46	0.196	[27]
Zn-graphene	− 1.16	2.36	0.230	
Cu-graphene	− 1.15	2.42	0.235	
Ni-graphene	1.846	1.692	0.208	[25]
Pd-graphene	1.228	2.202	−0.112	
Pt-graphene	1.858	2.353	−0.113	
Mn-graphene	− 4.3228	2.273	+0.171	[23]
Zn-ZGNR	− 2.237	2.70	− 0.037	Current work
Cu-ZGNR	− 1.129	2.75	− 0.059	
Cu/Zn-ZGNR	− 7.043	2.23	− 0.311	

the left and right electrodes are set to be 5.0 Å. The influence of doping and co-doping ZGNR with Cu and Zn atoms is firstly investigated as shown in Fig. 6(b). The result show that the pristine ZGNR reflect the highest current, while the current decrease dramatically for the cases of Zn-ZGNR, Cu-ZGNR, and Cu/Zn-ZGNR devices. Furthermore, the response of the proposed ZGNR, Zn-ZGNR, Cu-ZGNR, and Cu/Zn-ZGNR sensors toward H_2S is calculated with the aid of the I(V) curves as shown in Fig. 6(c). The results reveal that the response toward H_2S dramatically increases after substituting the Zn and Cu atoms into the surface of ZGNR. The slight response that has been obtained for the case of pristine ZGNR is mostly attributed to the slight changes of the electronic properties of the system as a result of the weak interaction (physisorption) of the H_2S molecule on its surface. More precisely, the response of the developed sensors to the H_2S molecules is found to be following the order ZGNR ‹ Zn-ZGNR ‹ Cu-ZGNR ‹ Cu/Zn-ZGNR as clearly indicated in Fig. 6(c). This order can be rationalized since both Zn and Cu based nanoparticles exhibit higher affinity (as compared with graphene) toward H_2S gas, with the higher affinity for the Cu based nanoparticles [18,19,38,47].

It's well known that the electronegativity of carbon atoms (2.55) is relatively high when compared with the copper (1.90) and zinc (1.65) metals. Therefore, carbon atoms located close to the position of the copper and zinc atoms gain more charges from them. Because of the charge transfer that has been demonstrated from H_2S to the doped and co-doped ZGNR systems, further rise in the charged state of the copper and zinc atoms occurs. This will result in enhancement of the reactivity of the surface that leads to stronger adsorption of the H_2S gas on the developed systems [27] demonstrated by the high adsorption energy, charge transfer, and electrical gas response of the co-doped ZGNR systems. Finally, a comparison between the adsorption energy, adsorption distance, and charge transfer results of the adsorption of the poisonous H_2S gas on different modified graphene systems is described in Table 3. As demonstrated in Table 3, the adsorption energies that are obtained for the case of H_2S/Cu/Zn-ZGNR system is significantly higher than the majority of the recent reports. Consequently, the developed Cu/Zn-ZGNR system can be considered as promising gas sensor for the effective sensing of the H_2S gas molecules.

4. Conclusion

In conclusion, first principles calculations have been performed on the impact of metal/metal co-doping on the sensitivity of zigzag graphene nanoribbon (ZGNR) towards the detection of the poisonous H_2S gas. Specifically, Cu and Zn metals have been substituted on the surface of ZGNR producing the proposed Cu/Zn-ZGNR sensors and then used to detect H_2S. The adsorption parameters as well as the response of the proposed Cu/Zn-ZGNR sensor toward H_2S were compared with both pristine and doped systems: ZGNR, Zn-ZGNR, and Cu-ZGNR. Intriguingly, the charge transfer as well as the adsorption energy of the H_2S/Cu/Zn-ZGNR system revealed an outstanding increase with respect to the other H_2S/ZGNR, H_2S/Zn-ZGNR, and H_2S/Cu-ZGNR systems. More precisely, the charge transfer and the adsorption energy of H_2S/Cu/Zn-ZGNR were found to be almost 14 and 19 times, respectively, larger than the case of H_2S/ZGNR. Furthermore, the impact of H_2S adsorption on the electronic properties as well as the electron transport demonstrated noticeable variations as compared with nearly invisible variations for the case of pristine ZGNR. Consequently, the metal/metal co-doping of graphene based materials would be suggested as an efficient tool to improve their accomplishment in the area of gas sensing of toxic gases.

Author statment

Ehab Salih: Visualization, Investigation, Writing- Original draft preparation. Ahmad I. Ayesh: Conceptualization, Methodology, Software, Supervision, Writing- Reviewing and Editing.

Declaration of competing interest

The authors declare that they have no known competing financial interests or personal relationships that could have appeared to influence the work reported in this paper.

Acknowledgements

Appendix A. Supplementary data

Supplementary data to this article can be found online at https://doi.org/10.1016/j.spmi.2021.106900.

References

[1] F. Schedin, A.K. Geim, S.V. Morozov, E. Hill, P. Blake, M. Katsnelson, K.S. Novoselov, Detection of individual gas molecules adsorbed on graphene, Nat. Mater. 6 (2007) 652–655.
[2] H.-p. Zhang, X.-g. Luo, X.-y. Lin, X. Lu, Y. Leng, H.-t. Song, Density functional theory calculations on the adsorption of formaldehyde and other harmful gases on pure, Ti-doped, or N-doped graphene sheets, Appl. Surf. Sci. 283 (2013) 559–565.

[3] A.I. Ayesh, Z. Karam, F. Awwad, M.A. Meetani, Conductometric graphene sensors decorated with nanoclusters for selective detection of Hg2+ traces in water, Sensor. Actuator. B Chem. 221 (2015) 201–206.

[4] K.S. Kim, Y. Zhao, H. Jang, S.Y. Lee, J.M. Kim, K.S. Kim, J.-H. Ahn, P. Kim, J.-Y. Choi, B.H. Hong, Large-scale pattern growth of graphene films for stretchable transparent electrodes, Nature 457 (2009) 706–710.

[5] F. Xia, T. Mueller, Y.-m. Lin, A. Valdes-Garcia, P. Avouris, Ultrafast graphene photodetector, Nat. Nanotechnol. 4 (2009) 839–843.

[6] K.I. Bolotin, F. Ghahari, M.D. Shulman, H.L. Stormer, P. Kim, Observation of the fractional quantum Hall effect in graphene, Nature 462 (2009) 196–199.

[7] A.H. Pourasl, M.T. Ahmadi, M. Ismail, N. Gharaei, Gas adsorption effect on the graphene nanoribbon band structure and quantum capacitance, Adsorption 23 (2017) 767–777.

[8] L. Shao, G. Chen, H. Ye, H. Niu, Y. Wu, Y. Zhu, B. Ding, Sulfur dioxide molecule sensors based on zigzag graphene nanoribbons with and without Cr dopant, Phys. Lett. 378 (2014) 667–671.

[9] B. Huang, Z. Li, Z. Liu, G. Zhou, S. Hao, J. Wu, B.-L. Gu, W. Duan, Adsorption of gas molecules on graphene nanoribbons and its implication for nanoscale molecule sensor, J. Phys. Chem. C 112 (2008) 13442–13446.

[10] E. Salih, A.I. Ayesh, Pt-doped armchair graphene nanoribbon as a promising gas sensor for CO and CO2: DFT study, Phys. E Low-dimens. Syst. Nanostruct. (2020) 114418.

[11] E. Salih, A.I. Ayesh, Computational study of metal doped graphene nanoribbon as a potential platform for detection of H2S, Mater. Today Comm. (2020) 101823.

[12] M. Haroon Rashid, A. Koel, T. Rang, First principles simulations of phenol and methanol detector based on pristine graphene nanosheet and armchair graphene nanoribbons, Sensors 19 (2019) 2731.

[13] S.K. Gupta, G.N. Jaiswal, Study of Nitrogen terminated doped zigzag GNR FET exhibiting negative differential resistance, Superlattice. Microst. 86 (2015) 355–362.

[14] A. Wasfi, F. Awwad, A.I. Ayesh, Electronic signature of DNA bases via Z-shaped graphene nanoribbon with a nanopore, Biosens. Bioelectron. X 1 (2019) 100011.

[15] Z. Ding, J. Jiang, H. Xing, H. Shu, R. Dong, X. Chen, W. Lu, Transport properties of graphene nanoribbon-based molecular devices, J. Computat. Chem. 32 (2011) 737–741.

[16] N.K. Jaiswal, G. Kovačević, B. Pivac, Reconstructed graphene nanoribbon as a sensor for nitrogen based molecules, Appl. Surf. Sci. 357 (2015) 55–59.

[17] U. Shefa, M.-S. Kim, N.Y. Jeong, J. Jung, Antioxidant and cell-signaling functions of hydrogen sulfide in the central nervous system, Oxidat. Med. Cell. Longev. (2018) 2018.

[18] A.I. Ayesh, A.F. Abu-Hani, S.T. Mahmoud, Y. Haik, Selective H2S sensor based on CuO nanoparticles embedded in organic membranes, Sensor. Actuator. B Chem. 231 (2016) 593–600.

[19] A.I. Ayesh, R.E. Ahmed, M.A. Al-Rashid, R.A. Alarrouqi, B. Saleh, T. Abdulrehman, Y. Haik, L.A. Al-Sulaiti, Selective gas sensors using graphene and CuO nanorods, Sensor Actuator Phys. 283 (2018) 107–112.

[20] V.A. Ranea, P.L.D. Quiña, N.M. Yalet, General adsorption model for H2S, H2Se, H2Te, NH3, PH3, AsH3 and SbH3 on the V2O5 (0 0 1) surface including the van der Waals interaction, Chem. Phys. Lett. 720 (2019) 58–63.

[21] H. Suman, R. Srivastava, S. Shrivastava, A. Srivastava, A. Jacob, C. Malvi, DFT analysis of H2S adsorbed zigzag and armchair graphene nanoribbons, Chem. Phys. Lett. (2020) 137280.

[22] E. Salih, A.I. Ayesh, DFT Investigation of H2S Adsorption on Graphenenanosheets and Nanoribbons: Comparative Study, Superlattices and Microstructures, 2020, p. 106650.

[23] X. Jia, H. Zhang, Z. Zhang, L. An, First-principles investigation of vacancy-defected graphene and Mn-doped graphene towards adsorption of H2S, Superlattice. Microst. 134 (2019) 106235.

[24] D. Cortés-Arriagada, N. Villegas-Escobar, D.E. Ortega, Fe-doped graphene nanosheet as an adsorption platform of harmful gas molecules (CO, CO2, SO2 and H2S), and the co-adsorption in O2 environments, Appl. Surf. Sci. 427 (2018) 227–236.

[25] Z. Bo, X. Guo, X. Wei, H. Yang, J. Yan, K. Cen, Density functional theory calculations of NO2 and H2S adsorption on the group 10 transition metal (Ni, Pd and Pt) decorated graphene, Phys. E Low-dimens. Syst. Nanostruct. 109 (2019) 156–163.

[26] S. Yang, G. Lei, H. Xu, B. Xu, H. Li, Z. Lan, Z. Wang, H. Gu, A DFT study of CO adsorption on the pristine, defective, In-doped and Sb-doped graphene and the effect of applied electric field, Appl. Surf. Sci. 480 (2019) 205–211.

[27] Z. Khodadadi, Evaluation of H2S sensing characteristics of metals–doped graphene and metals-decorated graphene: insights from DFT study, Phys. E Low-dimens. Syst. Nanostruct. 99 (2018) 261–268.

[28] J.P. Perdew, K. Burke, M. Ernzerhof, Generalized gradient approximation made simple, Phys. Rev. Lett. 77 (1996) 3865.

[29] S. Grimme, Semiempirical GGA-type density functional constructed with a long-range dispersion correction, J. Comput. Chem. 27 (2006) 1787–1799.

[30] S. Wang, B. Yang, E. Ruckenstein, H. Chen, Bco-C24: a new 3D Dirac nodal line semi-metallic carbon honeycomb for high performance metal-ion battery anodes, Carbon 159 (2020) 542–548.

[31] C. Zha, D. Wu, X. Gu, H. Chen, Triple-phase interfaces of graphene-like carbon clusters on antimony trisulfide nanowires enable high-loading and long-lasting liquid Li2S6-based lithium-sulfur batteries, J. Energy Chem. 59 (2021) 599–607.

[32] S. Wang, B. Yang, H. Chen, E. Ruckenstein, Popgraphene: a new 2D planar carbon allotrope composed of 5–8–5 carbon rings for high-performance lithium-ion battery anodes from bottom-up programming, J. Mater. Chem. 6 (2018) 6815–6821.

[33] D.C. Liu, J. Nocedal, On the limited memory BFGS method for large scale optimization, Math. Program. 45 (1989) 503–528.

[34] D. Liu, Y. Gui, C. Ji, C. Tang, Q. Zhou, J. Li, X. Zhang, Adsorption of SF6 decomposition components over Pd (1 1 1): a density functional theory study, Appl. Surf. Sci. 465 (2019) 172–179.

[35] E. Salih, A.I. Ayesh, CO, CO2, and SO2 detection based on functionalized graphene nanoribbons: first principles study, Phys. E Low-dimens. Syst. Nanostruct. (2020) 114220.

[36] R.S. Mulliken, Electronic population analysis on LCAO–MO molecular wave functions. I, J. Chem. Phys. 23 (1955) 1833–1840.

[37] M. Büttiker, Y. Imry, R. Landauer, S. Pinhas, Generalized many-channel conductance formula with application to small rings, Phys. Rev. B 31 (1985) 6207.

[38] A.I. Ayesh, A.A. Alyafei, R.S. Anjum, R.M. Mohamed, M.B. Abuharb, B. Salah, M. El-Muraikhi, Production of sensitive gas sensors using CuO/SnO 2 nanoparticles, Appl. Phys. A 125 (2019) 550.

[39] A.F. Abu-Hani, S.T. Mahmoud, F. Awwad, A.I. Ayesh, Design, fabrication, and characterization of portable gas sensors based on spinel ferrite nanoparticles embedded in organic membranes, Sensor. Actuator. B Chem. 241 (2017) 1179–1187.

[40] A.F. Abu-Hani, F. Awwad, Y.E. Greish, A.I. Ayesh, S.T. Mahmoud, Design, fabrication, and characterization of low-power gas sensors based on organic-inorganic nano-composite, Org. Electron. 42 (2017) 284–292.

[41] X. Gao, Q. Zhou, J. Wang, L. Xu, W. Zeng, Adsorption of SO2 Molecule on Ni-Doped and Pd-Doped Graphene Based on First-Principle Study, Applied Surface Science, 2020, p. 146180.

[42] E. Salih, A.I. Ayesh, Enhancing the sensing performance of zigzag graphene nanoribbon to detect NO, NO2, and NH3 gases, Sensors 20 (2020) 3932.

[43] Y.-W. Son, M.L. Cohen, S.G. Louie, Energy gaps in graphene nanoribbons, Phys. Rev. Lett. 97 (2006) 216803.

[44] V.E.C. Padilla, M.T.R. de la Cruz, Y.E.Á. Alvarado, R.G. Díaz, C.E.R. García, G.H. Cocoletzi, Studies of hydrogen sulfide and ammonia adsorption on P-and Si-doped graphene: density functional theory calculations, J. Mol. Model. 25 (2019) 94.

[45] G.K. Walia, D.K.K. Randhawa, First-principles investigation on defect-induced silicene nanoribbons—a superior media for sensing NH3, NO2 and NO gas molecules, Surf. Sci. 670 (2018) 33–43.

[46] E. Salih, A.I. Ayesh, First principle investigation of H2Se, H2Te and PH3 sensing based on graphene oxide, Phys. Lett. (2020) 126775.

[47] M.A. Haija, M. Chamakh, I. Othman, F. Banat, A.I. Ayesh, Fabrication of H 2 S gas sensors using Zn x Cu 1-x Fe 2 O 4 nanoparticles, Appl. Phys. A 126 (2020) 1–9.

[48] O. Faye, A. Raj, V. Mittal, A.C. Beye, H2S adsorption on graphene in the presence of sulfur: a density functional theory study, Comput. Mater. Sci. 117 (2016) 110–119.

[49] X. Gao, Q. Zhou, J. Wang, L. Xu, W. Zeng, Performance of intrinsic and modified graphene for the adsorption of H2S and CH4: a DFT study, Nanomaterials 10 (2020) 299.